The Design of an Onboard Digital Doppler Processor for a Spaceborne Scatterometer

DAVID G. LONG, CHONG-YUNG CHI, MEMBER, IEEE, AND FUK K. LI

Abstract—**The Seasat scatterometer (SASS) demonstrated the ability to infer near sea surface wind vectors from space [3]. The fixed-frequency analog filters employed in SASS did not compensate for the Doppler shift induced by the Earth's rotation and led to performance degradation and loss of swath. A digital Doppler processor, which will permit the Doppler center frequency of the measurement cell bandwidths to be adjusted to compensate for the effects of the Earth's rotation, will be used on the next NASA spaceborne scatterometer known as NSCAT. This paper describes the design and genesis of the NSCAT digital Doppler processor and discusses the performance trade-off issues that were critically evaluated during the design phase. This discussion will be of value to the designers of other related radar remote-sensing instruments.**

I. INTRODUCTION

A SCATTEROMETER is a radar system that measures the radar backscatter coefficient σ° of an illuminated surface [1]. The scatterometer transmits a series of RF pulses and measures the power of the backscattered signal that is corrupted by noise. A separate measurement of the noise-only power is subtracted from this measurement to yield the return signal power. Using the well-known radar equation and the measurement geometry, the backscattered power measurements are converted into σ° measurements [1]. Over the ocean, σ° measurements from multiple azimuth angles can be combined to infer near-surface wind vector [2].

The proof-of-concept Seasat scatterometer (SASS) operated for three months in 1978 until the spacecraft power system failed [3]. The data collected during this brief period clearly demonstrated that winds over the ocean could be accurately observed from space [3]. The success of SASS has prompted the development of the second-generation spaceborne scatterometers.

The signal processing for the Seasat scatterometer was performed using analog hardware that employed fixed-frequency bandpass filters for signal power estimation (diagrammed in Fig. 1). The bandpass filters had fixed center frequencies and bandwidths and could not compensate for the effects of the Earth's rotation. This led to performance degradation and loss of swath (see the illustration in Fig. 2). Following the end of the Seasat mission, NASA's Langley Research Center conducted a conceptual design study for a scatterometer to fly on the National Ocean Sensing System mission (NOSS) [4]. While never built, the proposed NOSS scatterometer design incorporated a digital Doppler processor to compensate for the Doppler shift induced by the Earth's rotation.

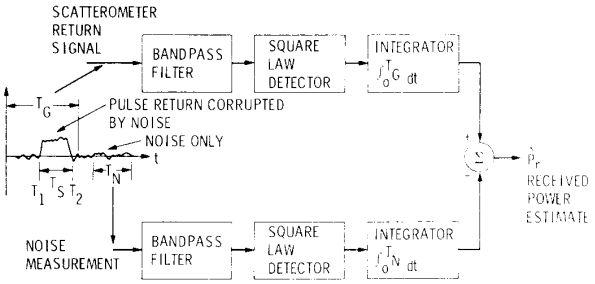

Fig. 1. Signal flow diagram for the Seasat scatterometer.

In 1983 NASA began a program to develop a spaceborne scatterometer to be flown in the early 1990's. The NASA Scatterometer (NSCAT) would be based primarily on design heritage from SASS with an advanced digital processor similar to the one proposed by the NOSS study.

A number of the design concepts developed during the design study for NOSS were incorporated into the NSCAT design. In particular, the NOSS study suggested that an FFT-based filtering technique could be used to provide the flexibility required to allow change of the Doppler measurement cell center frequencies to compensate for the Earth's rotation and maintain the σ° cells at a nearly constant cross-track distance from the spacecraft ground track. An additional advantage to this approach is that the Doppler parameters for the σ° cells can be adjusted for variations in orbit parameters due to launch errors or in-orbit maneuvers. Thus, the design of NSCAT incorporated a digital Doppler processor (DDP) for processing the radar return.

This paper discusses the design of the DDP for NSCAT. The paper is organized as follows: we describe general background needed for the design of onboard signal processors for spaceborne scatterometers, and discuss the rationale for using an FFT-based digital Doppler processor in Section II. In Section III we describe the design and tradeoff issues considered during the development of a digital Doppler processor for NSCAT. Finally, we summarize our conclusions.

Manuscript received March 25, 1987; revised March 28, 1988. This work was supported by the Jet Propulsion Laboratory, California Institute of Technology, under contract with the National Aeronautics and Space Administration.

The authors are with the Jet Propulsion Laboratory, Pasadena, CA 91109.

IEEE Log Number 8823160.

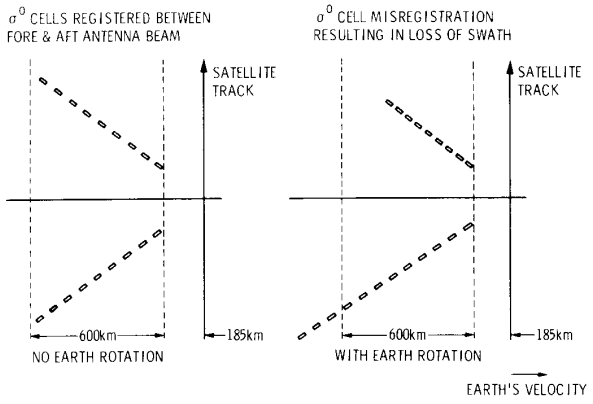

Fig. 2. An illustration of the σ° cell mis-registration effects due to the Earth's rotation when fixed-frequency filters are used.

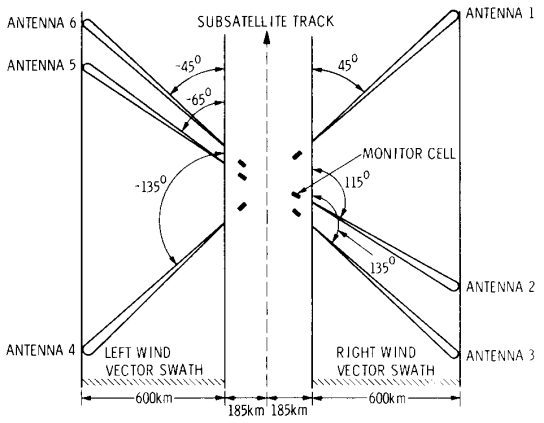

Fig. 3. NSCAT antenna illumination pattern on the ocean's surface.

II. General Design Issues for an Onboard Signal Processor for a Spaceborne Scatterometer

A. Measurement Resolution

In the NSCAT designs, six fan-beam antennas provide the surface illumination patterns shown in Fig. 3 [5]. The center beams provide additional "skill" for determining the unique wind direction from the σ° measurements [6]. The illumination pattern is designed so that a given portion of the ocean's surface is first observed by a forward antenna to provide a σ° measurement from one azimuth angle, then, as the spacecraft moves along the ground track, by the center antenna for a second azimuth angle, followed by the aft antenna for the third azimuth angle. The σ° measurements from the three different azimuth angles are combined by ground processing to infer the vector wind. The narrow antenna illumination pattern and the measurement timing provide the along-track resolution.

The transmitted radar signal reflected from the ocean's surface is Doppler shifted due to the relative motion of the Earth's surface and spacecraft. The return echo from different portions along the antenna illumination pattern have different Doppler shifts and can be separated into cross-track resolution elements known as "σ° cells" by Doppler bandpass filtering.

While cross-track resolution is obtained by Doppler filtering, along-track resolution is achieved by the time interval between measurements. As the spacecraft moves along its ground track, the σ° cells viewed by each of the antenna beams in sequence are sampled once during the time interval required for the spacecraft to move the along-track sampling distance (25 km for NSCAT).

B. Radar Return Signal Characteristics

A typical Doppler-shifted time-history (Doppler history) of the scatterometer return signal from a forward antenna is shown in Fig. 4. The return echo time-interval and bandwidth of the return echo from each of the σ° cells is indicated as a boxed region. Time is relative to the start of transmit pulse.

The scatterometer return signal has a number of important characteristics that affect the design and analysis of the Doppler filter. The following observations about the Doppler history are relevant: 1) cells close to the subsatellite ground track (in the near swath region) have a smaller Doppler shift than cells in the far swath region, 2) far swath cells require less bandwidth than near swath cells, and 3) the time-of-flight for the return signal is longer for far swath cells.

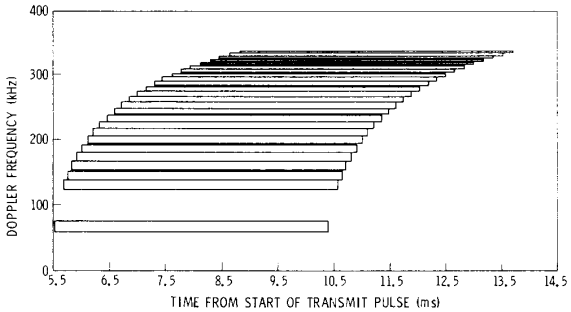

Fig. 4. Typical Doppler history for the radar echo return from a forward-looking antenna. Boxed regions indicate σ° cell time/bandwidth regions.

The scatterometer return signal from other antenna beams is similar to the above but: 1) the Doppler shift of aft-facing antennas is reversed in sign from the forward-facing antennas and 2) the return signal from the center antennas is similar to the fore and aft antennas but has a smaller Doppler/time spread.

C. Doppler Shift for a Constant Cross-Track Distance

To maintain each of the σ° cells at a fixed cross-track distance from the spacecraft track as the spacecraft moves along its orbit, the Doppler shift of the σ° cells must be changed to compensate for the effects of the Earth's rotation. An example of the change in center frequency of the σ° cells as a function of the time from the northbound equator crossing (ascending node) is shown in Fig. 5. Note the nearly sinusoidal variation in center frequency as a function of time.

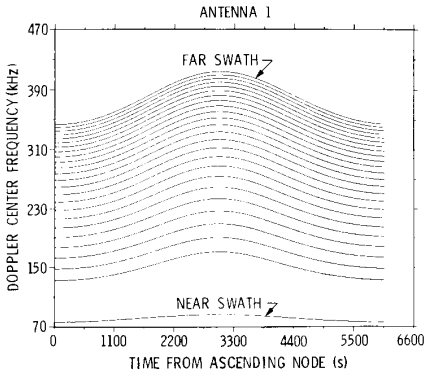

Fig. 5. Doppler shift center frequencies of typical σ° cells as a function of the time from the ascending node equator crossing.

Not only do the cell center frequencies change, but the return echo time-of-flight also changes. In order to adequately process the scatterometer return signal the Doppler processor must consider the entire time/bandwidth spanned by all σ° cell bandwidths as the center frequencies vary over the orbit. For the NSCAT design, this corresponds to a bandwidth of approximately ± 400 kHz with a time-of-flight of between 5.5 and 11 ms (assuming an orbital altitude of 820 km).

D. Digital Doppler Processor

The design considerations and signal characteristics discussed above have led to the use of a digital Doppler processor (DDP) for NSCAT rather than an analog processor. The use of a digital processor has several advantages: 1) the signal processing required to measure the return echo power can be done more accurately using digital hardware, 2) the digital approach can easily vary the center frequencies of σ° cells as a function of the spacecraft position along its orbit, and 3) the digital processor also permits changing of the σ° cell bandwidths and center frequencies in response to changing orbit conditions (e.g., orbit decay).

E. Performance Evaluation of the Signal Processor

The scatterometer measures the return echo power P_r from the ocean's surface. The measurement accuracy for P_r depends on the noise power due to thermal effects in the receiver and antennas. A commonly adopted parameter for evaluating the performance of spaceborne scatterometers is the so-called K_p parameter [7], which is defined as the normalized standard deviation of the measured σ°, σ°, or $\hat{P}_r$

$$K_p = \frac{\{\text{Var}\,[\hat{P}_r]\}^{1/2}}{P_r} = \frac{\{\text{Var}\,[\sigma^\circ]\}^{1/2}}{\sigma^\circ}. \quad (1)$$

K_p is an indicator of how accurate the σ° measurement is. A general goal in scatterometer design is to minimize K_p. The equation for the K_p of an analog Doppler processor, such as that used on SASS, is [7]

$$K_p = \frac{1}{\sqrt{B_S T_S}}\left\{1 + \frac{2}{\text{SNR}} + \frac{1}{\text{SNR}^2}\left(1 + \frac{T_G B_S}{T_N B_N}\right)\right\}^{1/2} \quad (2)$$

where B_S is the bandwidth of the σ° measurement cell, T_G is the integration time length, SNR is the signal-to-noise ratio, T_S is the length of the echo return signal, T_N is the noise measurement time, and B_N is the noise measurement bandwidth (see Fig. 1) [7]. In order to perform design tradeoff studies, an equivalent expression for the K_p of the FFT-based digital processor was derived in an earlier paper [8]. The equation is given by (8) below.

F. Other Design Considerations

Since, for a given antenna, the Doppler shift of the measurement cells is either all positive or all negative, the processing bandwidth requirements on the digital processor can be reduced to processing only positive "Doppler" shifts by using RF mixing in the receiver, which changes the sign of negative Doppler shifts to positive Doppler shifts. This RF mixing step will be termed spectral reversal since the net effect of the sign change of the Doppler shift is to reverse (with respect to zero Doppler shift) the Doppler spectrum.

III. Design Issues for FFT-Based Digital Doppler Processors

Before considering the design issues for the DDP, let us briefly consider the measurement sequence and timing, which defines the along-track resolution, and the type of RF signal sampling employed to provide the input to the DDP.

A. Measurement Sequence and Timing

Each return echo power measurement consists of a series of transmit/receive cycles (refer to Fig. 6). The number and length of the transmit/receive cycles are driven by the time-of-flight of the transmit pulse and the return echo, the transmit pulse length, and the time between along-track measurements. The large difference (6 ms) between the time-of-flight for the return echo from the near and far swath has been noted. Based on this large difference a 5-ms CW transmit pulse followed by a receive period sufficient to receive the entire return from the far swath provides a simple architecture for both the digital and radio-frequency (RF) portions of the instrument design.

For the NSCAT design, the return echo signal plus noise power from 25 transmit pulses is individually accumulated from each of the 8 antenna beams in sequence to obtain the signal plus noise power measurements. After the signal plus noise power measurements are made on a particular antenna beam, a separate measurement of the noise-only power is made. A detailed timing diagram for NSCAT is shown in Fig. 6. The accumulated signal plus noise and noise-only power measurements are telemetered to the ground where the noise-only power measurements are subtracted from the signal plus noise power measurements to determine the signal power. The signal power measurements are then converted into σ° measurements using the radar equation [1].

B. RF Input Signal Sampling

The NOSS study proposed in-phase/quadrature (I/Q) sampling of the RF receiver output to minimize the digital

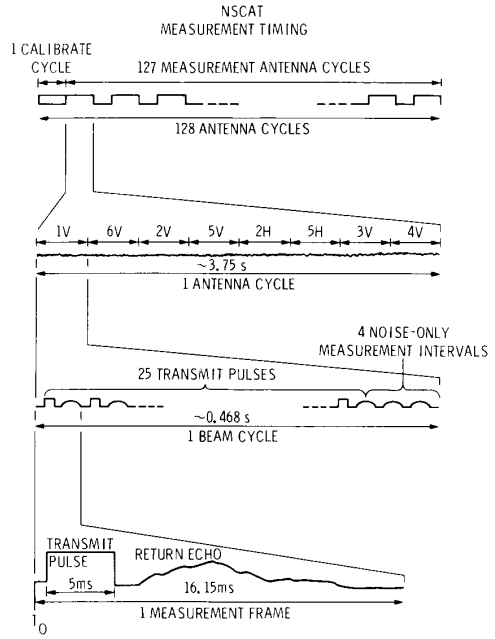

Fig. 6. NSCAT timing diagram and measurement sequence.

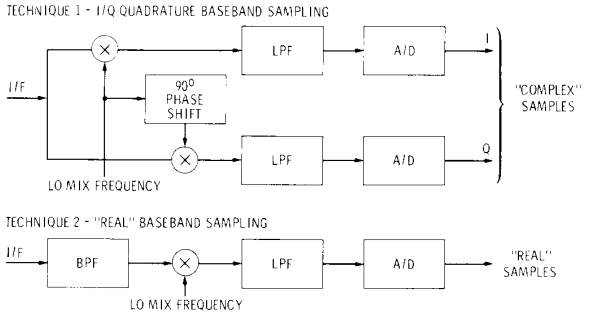

Fig. 7. Comparison of the RF mixing schemes used to provide complex I/Q baseband sampling and ordinary "real" sampling.

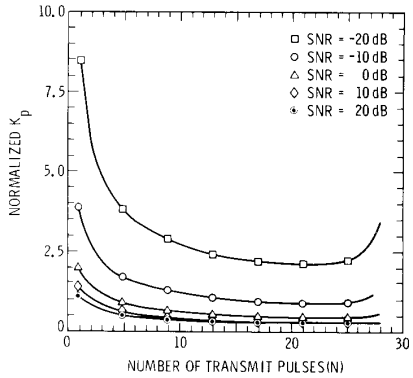

Fig. 8. K_p versus the number of transmit pulses used for power measurement. The plotted values have been normalized by the case for $N = 25$ transmit pulses with 4 receive "pulses" at an SNR value of 20 dB. The total number of pulses is fixed at 29.

hardware in the DDP. The I/Q sampling approach provides "complex" data samples as input to the FFT-based signal processor. I/Q sampling requires an RF power splitter, mixers, a 90-degree phase shifter, and two low-pass filters to produce the "complex" signal (see Fig. 7). Furthermore, the gain of each of the input paths must be carefully matched to avoid introducing artifacts and errors into the measured power.

The difficulties and additional RF hardware required for I/Q sampling can be avoided while still minimizing the computational load on the FFT processor by taking advantage of the even/odd symmetry properties of the FFT. With this technique the FFT of two "real" data segments are computed simultaneously by using one segment, $x_1(n)$, as the "real" part and the other, $x_2(n)$, as the "imaginary" part of the input $x(n) = x_1(n) + jx_2(n)$ to a complex FFT calculation. The result of the FFT, $X(k)$, can be "decomposed" into the Fourier transforms $X_1(k)$ and $X_2(k)$ of the inputs $x_1(n)$ and $x_2(n)$, respectively, using the formulae

$$2X_1(k) = \mathrm{Re}\,[X(k)] + \mathrm{Re}\,[X(-k)] + j\big(\mathrm{Im}\,[X(k)] - \mathrm{Im}\,[X(-k)]\big) \quad (3)$$

$$2X_2(k) = \mathrm{Im}\,[X(k)] + \mathrm{Im}\,[X(-k)] + j\big(\mathrm{Re}\,[X(-k)] - \mathrm{Re}\,[X(k)]\big). \quad (4)$$

This approach uses a longer FFT length than the I/Q sampling scheme, must have double the sample rate, and requires the additional digital decomposition stage during processing but eliminates the additional RF hardware required for I/Q sampling and the I and Q channel balance problem. This approach was adopted in the NSCAT design.

C. Signal Plus Noise and Noise-Only "Pulses"

To simplify the processor design, the noise-only power measurement was chosen to have timing similar to the signal plus noise measurement but with only 4 "pulses." No transmit pulse is actually issued but the noise power measured during the receive interval is accumulated as the noise-only measurement. The tradeoff between the number of transmit pulses and the number of noise-only measurement pulses was made by selecting the combination of signal plus noise and noise-only pulses that minimized K_p. Fig. 8 illustrates a plot of K_p versus the number of signal plus noise pulses where the total number of measurement "pulses" is 29. The value of K_p in Fig. 8 has been normalized by the value of K_p when 25 transmit pulses and 4 receive "pulses" are used at an SNR value of 20 dB. The 25/4 transmit-to-receive ratio provides near-optimum K_p performance.

During the noise-only measurement, the noise power over both the σ° cell bandwidths and the entire processing bandwidth is measured. The use of the wide-band noise measurement (B_N in (8)) permits the reduction in the number of noise-only pulses required to achieve a given K_p.

D. Signal Processing and K_p

The FFT-based Doppler filtering approach originally suggested by the NOSS study was chosen over an IIR or

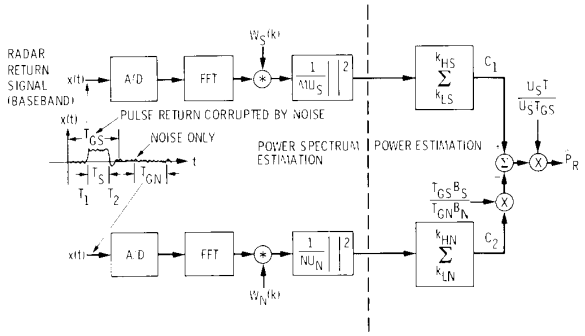

Fig. 9. Signal flow diagram for a FFT-based digital Doppler processor.

FIR approach since it provides a very simple method for adjusting the center frequencies of the σ° cell bandwidths and can be easily implemented in hardware. In an Infinite Impulse Response (IIR), or Finite Impulse Response (FIR) filter approach, a large number of filter coefficients for the bandpass filter on each cell must be determined each time the center frequency is varied. The amount of memory required to store the coefficients was considered excessive and precluded onboard storage. Furthermore, the amount of computation required to compute the coefficients in real-time onboard makes this approach not viable.

A signal flow diagram for the FFT-based digital signal processor is shown in Fig. 9. The processor provides measurements C_1 and C_2 of the signal plus noise power and noise-only power, respectively. The unbiased estimate $\hat{P}_r$ of backscattered signal power P_r is [8], [11]

$$\hat{P}_r = \frac{U_S T}{U_S^* T_{GS}} \left(C_1 - \frac{T_{GS} B_S}{T_{GN} B_N} C_2 \right) \tag{5}$$

where the measurements C_1 and C_2 are

$$C_1 = \frac{1}{K_S N_{PS} M U_S} \sum_{j=1}^{N_{PS}} \sum_{i=1}^{K_S} \sum_{k=k_{LS}}^{k_{HS}} \left| X_i^{(j)}(k) * W_S(k) \right|^2 \tag{6}$$

$$C_2 = \frac{1}{K_N N_{PN} N U_N} \sum_{j=1}^{N_{PN}} \sum_{i=1}^{K_N} \sum_{k=k_{LN}}^{k_{HN}} \left| X_i^{(j)}(k) * W_N(k) \right|^2 \tag{7}$$

where $X_i^{(j)}(k)$ is the Fourier transform of the $(i)^{\text{th}}$ data segment and the (j^{th}) pulse of the DDP input with the remaining parameters defined in Table I [8], [11].

In the FFT-based approach, a Welch's power spectrum estimate is provided by an FFT/periodogram processor [8]. This consists of 1) computing the FFT of the sampled input data segments, 2) application of a data window by convolution, 3) squaring (power detection) of the windowed FFT output, and 4) summing the resulting periodogram bins over the range of bins corresponding to the σ° cell bandwidth of interest. The center frequency can be changed by simply changing the range of bins summed. This approach permits power measurements for multiple cells to be computed simultaneously.

TABLE I
DIGITAL PROCESSOR K_p EQUATION PARAMETERS

Signal plus noise	Noise only	Description
T_{GS}	T_{GN}	Time interval of one data segment
B_S	B_N	Bandwidth
k_{LS}	k_{LN}	Lower frequency bin number
k_{HS}	k_{HN}	Upper frequency bin number
k_S	k_N	$k_{HS} - k_{LS} + 1$, $k_{HN} - k_{LN} + 1$
$w_S(n)$	$w_N(n)$	Window function (in time domain)
U_S	U_N	$U_S = \frac{1}{M}\sum_{n=0}^{M-1} w_S^2(n)$, $U_N = \frac{1}{N}\sum_{n=0}^{N-1} w_N^2(n)$
N_{PS}	N_{PN}	Number of measurement pulses
K_S	K_N	Number of data segments
M	N	Number of data points per segment $T_{GS}/T, T_{GN}/T$
D		Number of nonoverlapping data points in consecutive data segments
T		Sampling interval $= 1/f_S$
T_1		Signal start time
T_S		Signal pulse length
b'		Noise power spectral density
SNR		Signal-to-Noise ratio$=P_r/(B_S b')$
$W_S(q,k)$		Fourier transform of $w_S(n)w_S(n+qD)$
$W_N(q,k)$		Fourier transform of $w_N(n)w_N(n+qD)$
$\gamma_i(n)$		$\begin{cases} rect(nT + (i-1)DT - T_1)w_S(n), & \text{if } 0 \le n \le M-1; \\ 0, & \text{otherwise} \end{cases}$
$\gamma_{ij}(n)$		$\gamma_i(n)\gamma_j(n+(i-j)D)$
$\Gamma_{ij}(k)$		Fourier transform of $\gamma_{ij}(n)$
U_i		$\frac{1}{M}\sum_{n=0}^{M-1}\gamma_i^2(n)$
U_S^*		$\frac{1}{K_S}\sum_{i=1}^{K_S} U_i$
$rect(t)$		$\begin{cases} 1, & 0 \le t \le T_S; \\ 0, & \text{otherwise} \end{cases}$

The K_p expression for this processor is [8], [11]

$$K_p = \frac{1}{\sqrt{T_{GS} B_S}} \frac{1}{M U_S^*} \left\{ \frac{1}{K_S^2 N_{PS}} \sum_{k=-k_S}^{k_S} \sum_{i=1}^{K_S} \sum_{j=1}^{K_S} \left(1 - \frac{|k|}{K_S}\right) \cdot \left| \Gamma_{ij}(k) + \frac{1}{\text{SNR}} W_S(i-j,k) \right|^2 + \frac{1}{K_N N_{PN}} \frac{T_{GS} B_S}{T_{GN} B_N} \cdot \left(\frac{M U_S}{N U_N}\right)^2 \cdot \frac{1}{\text{SNR}^2} \left[\sum_{k=-k_N}^{k_N} \sum_{q=-K_N}^{K_N} \left(1 - \frac{k}{k_N}\right) \cdot \left(1 - \frac{|q|}{K_N}\right) |W_N(q,k)|^2 \right] \right\}^{1/2} \tag{8}$$

where all the parameters are described in Table I.

Several general statements can be made regarding the effect of the instrument design on the accuracy of the σ° measurements (K_p): 1) longer integration times $(T_{GS} N_{PS})$ reduce K_p and thus improve measurement accuracy, 2) wider measurement bandwidths reduce K_P, 3) K_p^2 is a quadratic function of the inverse of the SNR. These state-

ments also apply to the analog processor K_p equation given in (2).

E. Multichannel Signal Processing

The required frequency resolution of the DDP is driven by the required σ° cell resolution and location accuracy. To meet the NSCAT mission requirements [9], the maximum σ° cell location error must be less than 4-km cross-track distance. At the far swath, a 4-km cross-track error corresponds to a relative Doppler shift of approximately 200 Hz. At the near swath this corresponds to a Doppler shift of about 550 Hz. Using the FFT-based filtering approach, the cell center frequency, which determines the cell location on the ocean's surface, is limited to the discrete FFT bin center frequencies. This dictates that the frequency resolution of the FFT processor be at least 200 Hz for far swath cells and at least 550 Hz for near swath cells.

The sample rate and the number of points in the FFT (referred to as the FFT size) are driven by these frequency resolution requirements and the Doppler bandwidth spread of the σ° cells. For NSCAT the Doppler spread is approximately 400 kHz. A single processing channel with such a bandwidth and a frequency resolution would require a sampling rate greater than 800 kHz and an FFT size greater than 4000 points. However, the processing bandwidth can be split into multiple processing channels, each of which covers only part of the processing bandwidth to reduce the sample rate and FFT size. This approach, suggested in the NOSS study, reduces the sample rate, FFT size, and commensurate computational load. Furthermore, the difference in the frequency resolution required for near and far swath cells can be exploited to further reduce the sample rate and FFT size.

Division of the return signal into multiple channels for "real" sampling can be accomplished using the RF mixing scheme diagrammed in Fig. 10. In this example, the 410-kHz processing bandwidth is divided into two processing channels. The RF signal in each channel bandwidth is mixed down to the baseband where it can be digitally sampled. For this particular example, channel A has a bandwidth of 110 kHz (minimum sample rate required: 220 kHz) and channel B has a bandwidth of 300 kHz (minimum sample rate required: 600 kHz). The total processing bandwidth is 410 kHz. With an FFT size of only 1100 points, channel A could obtain a frequency resolution of 550 Hz while channel B would have a frequency resolution of 200 Hz.

Since the center frequencies of the σ° cells change as a function of the orbit, the σ° cells may move from one processing channel bandwidth to another. By requiring the channel bandwidths to overlap in frequency so that the σ° cell bandwidth is always completely contained within a single channel, computation of the cell power can be made within a single channel. This keeps the DDP design simple and does not require precise gain matching of the channels. The digital hardware design complexity can also be minimized by restricting the FFT size to a power of 2

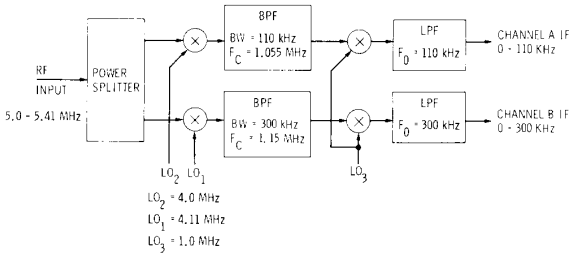

Fig. 10. An example illustrating the RF mixing scheme to provide multiple channel processing.

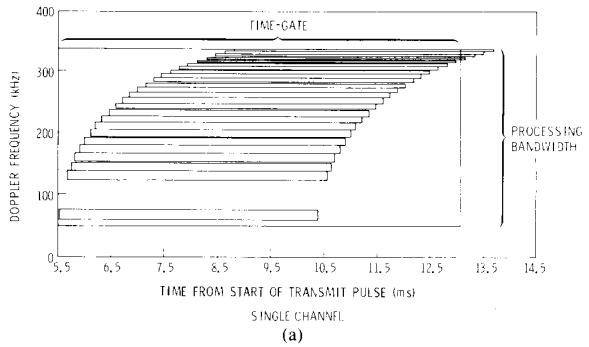

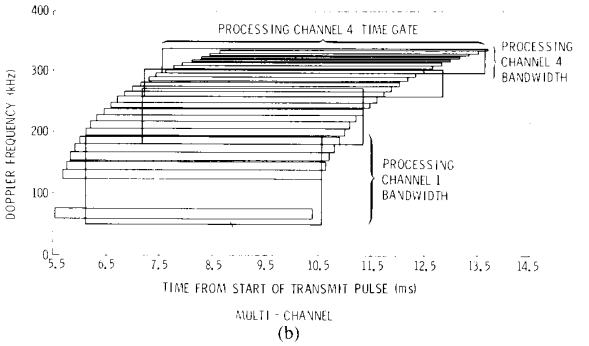

Fig. 11. A graphical comparison of the DDP time/bandwidth superimposed on a typical echo return Doppler history for (a) a single-channel design and (b) a multiple channel design.

and requiring the FFT size to be the same for all processing channels. This permits the same FFT hardware to be shared between channels.

Multiple processing channels permits separate time-gates on each of the channels so that the time-gate/bandwidth of the processor can "follow" the Doppler history of the signal to minimize the inclusion of additional noise in the power measurement. This is illustrated in Fig. 11 where the time/bandwidth of a single-channel processor is contrasted with that of a multichannel design. The inclusion of the noise time/bandwidth decreases the average signal to noise ratio of the measurement which results in increased K_p. Consider Fig. 12, which shows the value of K_p normalized by the equivalent analog K_p (termed the "ideal K_p") for each σ° cell across the swath for the par-

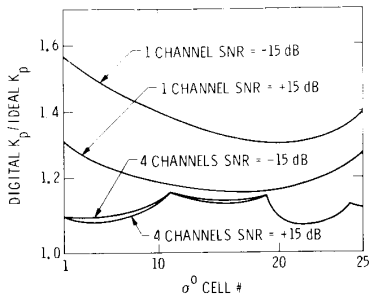

Fig. 12. K_p for a DDP versus cross-track σ° cell number for single-channel and multichannel processor designs. The value plotted has been normalized by the "ideal" analog K_p (see text).

ticular multichannel and single-channel DDP designs shown in Fig. 11.

The number of channels, the bandwidth of each channel, and the FFT size were selected after an exhaustive comparison of the K_p performance of each design and considering computational limitations on the hardware design. The result of this study was selection of a 4-channel design using 512 point FFT's for each channel. The bandwidths of these four channels were roughly in the proportion of 4 : 2 : 1 : 1.

F. Data Windowing

The sampled data is Fourier transformed and then a data window is applied in the frequency domain by convolution (see Fig. 9). The data window is required to reduce the interference between measurement bandwidth power measurements due to spectral leakage [10]. A measure of the performance of the data window in reducing undesired interference between measurement cells is the integrated sidelobe ratio (ISLR), which we define as the energy in the bandstop region (side lobe) of the window transform divided by the total energy of the window.

A generalized Hamming window was selected for the data window since it can be applied very efficiently by frequency domain convolution. A generalized Hamming window $w(n)$ of length N is defined as

$$w(n) = \alpha - (1 - \alpha) \cos (2\pi n/N) \qquad (9)$$

where $(0 \leq \alpha \leq 1)$ is the generalized Hamming window parameter. A value of $\alpha = 1$ corresponds to a rectangular window while $\alpha = 1/2$ corresponds to a Hann window. Fig. 13 shows a plot of the ISLR versus α for the generalized Hamming window with $N = 512$ the FFT size. While the use of a data window degrades the FFT bin spectral resolution, the degraded resolution is more than adequate to meet the cell location requirements.

In order to meet the NSCAT mission requirements for measurement error, the ISLR must be less than -30 dB. We note that when $\alpha = 1/2$ the coefficients of the window transform are fractional powers of two. This permits a particularly simple hardware implementation of the windowing operation while meeting the ISLR requirements. A value of $\alpha = 1/2$ was used in the NSCAT design.

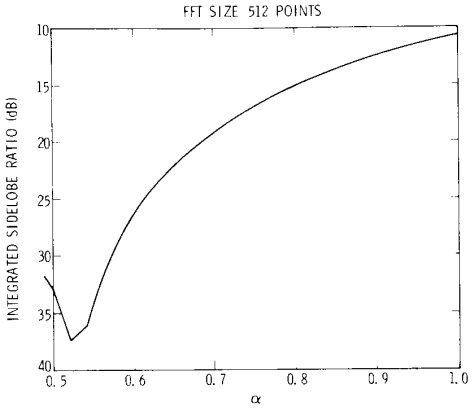

Fig. 13. Integrated sidelobe ratio (ISLR) for a generalized Hamming window versus the value of the window parameter α.

G. Time-Overlapped Processing

Although windowing is required to minimize cell-to-cell spectral interference, it adversely affects K_p performance. A plot of the $K_p(\alpha)$ computed using (8) versus α is shown in Fig. 14. The plotted $K_p(\alpha)$ has been normalized by $K_p(\alpha = 1)$. As α is decreased from 1 to 1/2, $K_p(\alpha)/K_p(\alpha = 1)$ increases from 1 to 1.4. The K_p degradation due to windowing can be minimized by the use of time-overlapped processing of the input data (see [8]) at the expense of additional computation. This is accomplished by taking time-overlapped segments of data, processing each with an FFT, windowing, squaring and summing the results (see (6) and (7)). An example illustrating the improvement in K_p due to time-overlapping when a Hann window is used is shown in Fig. 15, which gives $K_p(\alpha = 1/2)$ as a function of the data segment overlap. We note that K_p improves significantly as the overlap is increased from 0 to 50 percent but very little additional improvement is evident beyond 50 percent. Due to hardware limitations on the number of FFT's that could be computed in real-time onboard NSCAT, the time-overlap was limited to 50 percent.

H. Input Signal Time-Gating

The return echo is time-gated by sampling the receiver output signal only during the time interval that contains the return echo power. Each processing channel has a different time-gate start time and time-gate length to permit the time/bandwidth of the processor to "follow" the time/Doppler history of the processor (see Fig. 4) to minimize the value of K_p. The time-gate is opened at a time T_1 from the start of the transmit pulse and closed after the sampled data segments are filled. The length of the time gate is a function of the sample rate, the data segment length (which is the same as the FFT size), and the data segment overlap. The start time-gate is adjusted so that as much of the return echo from all of the σ° cells within the processing channel bandwidth as possible is within the time-gate.

During the early development of the NSCAT DDP de-

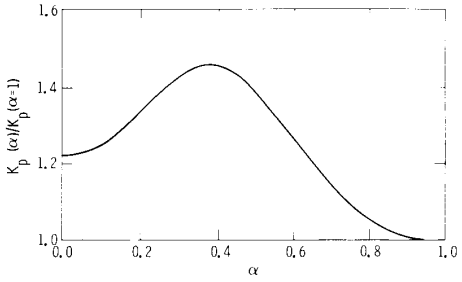

Fig. 14. $K_p(\alpha)$ versus the windowing parameter α for a single data segment. The value plotted has been normalized by $K_p(\alpha = 1)$ corresponding to a rectangular window.

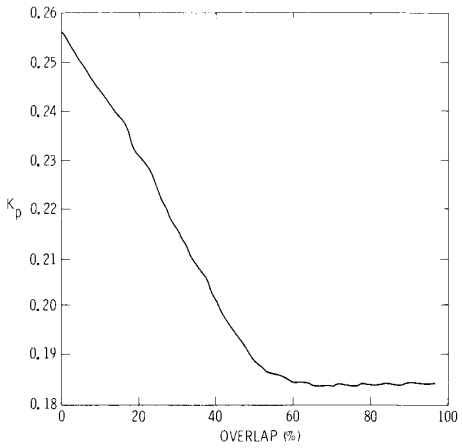

Fig. 15. $K_p(\alpha = 1/2)$ versus the percentage of data segment time-overlap.

TABLE II
NSCAT DIGITAL DOPPLER PROCESSOR DESIGN SUMMARY

σ° cell spacing	25 km
σ° cells on each side of swath	24
Channels	4
Approximate Channel Bandwidth Proportion	4:2:1:1
FFT Size	512 points
Generalized Hamming Window Parameter (α)	1/2
Data Segment Time-Overlap	50 %
Total Processing Bandwidth	450 kHz
Antennas Using Spectral Reversal	2,3,4

Channel Number	No. of FFT Segments	T_1 (ms)	Bandwidth kHz	Center Frequency kHz	Sample Frequency kHz
1	7	6.464	209.041	141.103	483.781
2	3	7.931	113.538	270.182	262.757
3	2	8.030	58.506	337.716	135.400
4	2	8.327	52.831	380.861	122.267

TABLE III
DIGITAL DOPPLER PROCESSOR IMPLEMENTATION SUMMARY—BITS PER STAGE (REFER TO FIG. 9)

DDP Processing Stage	Bits
A/D	8
FFT	16
Windowing	18
Squaring	32
Bin Summing	28
Output Floating-point exponent	4
Output Floating-point mantissa	12

sign, a large number of possible configurations of the number of channels, FFT size, sample rate, data segments (FFT's) per channel, channel bandwidth proportions, and time-gates were considered. These were ranked according to K_p performance, RF hardware required, and the required computation rate. As mentioned, a 4-channel design with bandwidth proportions 4:2:1:1 and 512 point FFT provided the best tradeoff in K_p performance and computational load. The number of overlapping data segments for each channel was 7:3:2:2 with a data segment overlap of 50 percent. The bandwidths of the channels were widened and overlapped to insure that each σ° cell bandwidth is always completely contained within a processing channel. The final design parameters for the NSCAT DDP are summarized in Table II.

I. Quantization, Finite Arithmetic, and Dynamic Range

Practical considerations in the implementation of digital signal processors include the conversion of analog signals to digital representation (quantization), type of arithmetic (fixed-point or floating-point), and word length at each stage of processing. The processor realization will be driven by the required dynamic range at each stage, computational limitations of available hardware, etc. Arithmetic error in computations (due to overflow, underflow, or word truncation) and the quantization error that occurs when the analog signal is converted to a digital representation degrades the accuracy of the power measurements.

The reader is referred to [11], [12] for a detailed discussion of these effects on the processor design for NSCAT and for a derivation of the errors due to quantization and arithmetic error. The results based on the tradeoff studies presented in [11] and [12] are summarized in Table III (see Fig. 9). The 28-bit accumulated power measurements at the output of the processor are converted to a 16-bit floating-point representation (12-bit mantissa, 4-bit exponent) for transmission to the ground.

J. "Binning" Algorithm

The σ° cell power measurement is made by summing a specified range of periodogram bins in the signal processor. The range of bins summed into each cell's power measurement is determined using a "binning" algorithm. The binning algorithm specifies the center frequency of each σ° cell in order to maintain the σ° cells at the same cross-track distance as a function of the orbit. The amount of memory required to store the σ° cell center frequencies for all beams and orbit times was considered excessive. This has led to the decision to compute the σ° cell center frequencies in real-time onboard the spacecraft.

The expression relating the cell location to its Doppler

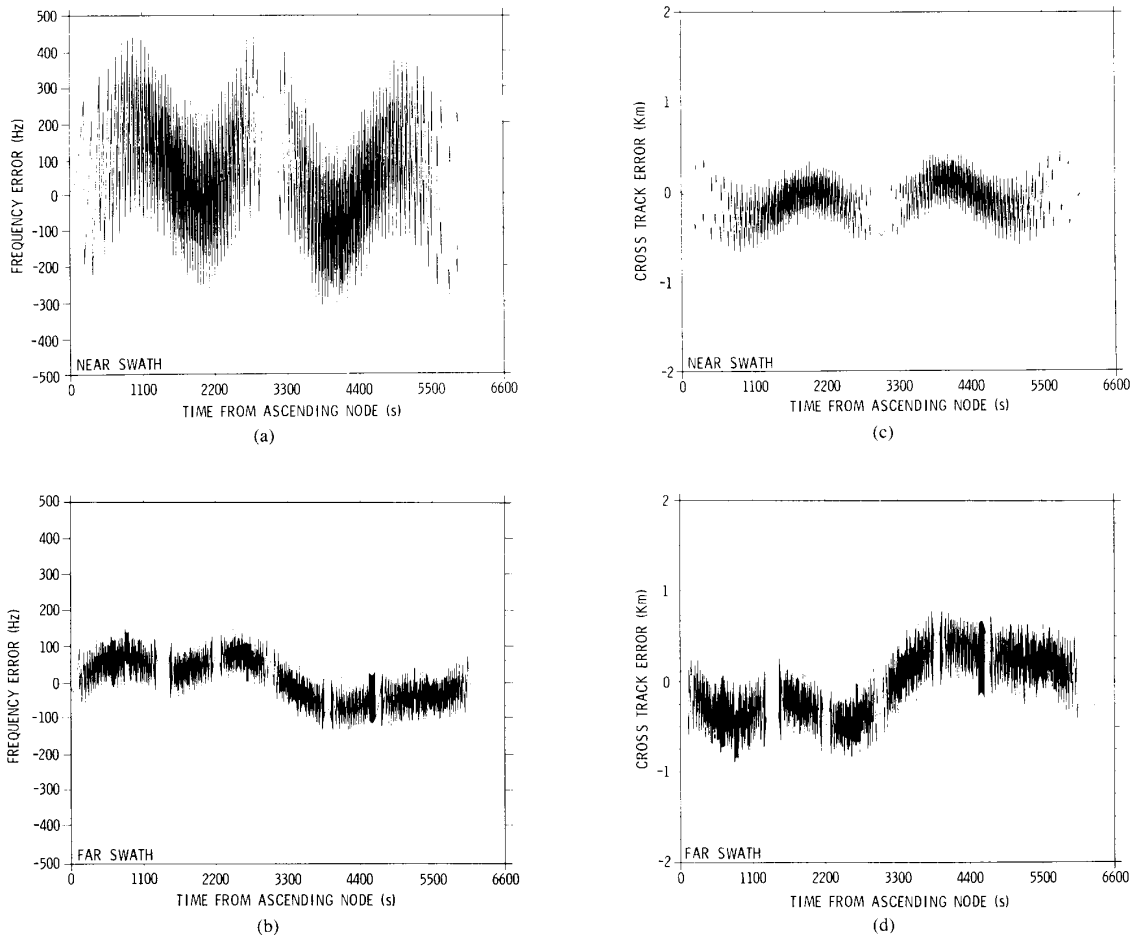

Fig. 16. Center frequency error for (a) near and (b) far swath σ° cells error for the onboard binning algorithm versus the time from ascending node (north bound equator crossing). σ° cell cross-track distance error for (c) near and (d) far swath resulting from the frequency error. The orbit period is approximately 6100 s.

shift as a function of the orbit is quite complex and generally unsuited for onboard computation. Instead, a number of functional approximations were considered including polynomial fits and Fourier expansions. These were ranked by the root mean square (rms) error between the σ° cell cross-track location based on the approximated Doppler shift and the ideal σ° cell cross-track location. A truncated Fourier series expansion provided an excellent tradeoff between computational complexity and rms cross-track error. This approximation consisted of the first three terms in the Fourier series expansion of the σ° cell center frequency $F_c(t)$ as a function of time from the ascending node (northbound equator crossing) t

$$F_c(t) = A_0 + A_1 \cos(P_d t + \phi_1) + A_2 \cos(2P_d t + \phi_2) \quad (10)$$

where A_0, A_1, A_2, ϕ_1, ϕ_2 are constants and $P_d = 2\pi/P$ where P is the orbit period. This equation can be easily computed on-board by using a cosine-value lookup table stored in ROM. The binning constants A_0, A_1, A_2, ϕ_1, ϕ_2 and the cell bandwidth can be stored in onboard RAM. This permits modification of the binning constants to accommodate changes in the spacecraft orbit to maintain constant σ° cell cross-track locations.

The form of the truncated Fourier series approximation is robust with respect to changes in the orbit, that is, only the constants A_0, A_1, A_2, ϕ_1, ϕ_2 and perhaps P_d need to be changed as the orbit changes to maintain the σ° cells at a constant cross-track distance from the subsatellite ground track. Fig. 16 illustrates the frequency error and the resulting σ° cell cross-track distance error inherent in the algorithm and DDP design for the baseline NSCAT nearly circular, polar orbit (inclination angle 98.7 degrees, altitude 820 km). Quantization evident in the plot is due to the discrete nature of the FFT bin center frequencies.

For NSCAT, the binning algorithm will be implemented in software. In addition to computing the cell center frequency, the software will determine which channel

completely contains each σ° cell bandwidth. The center frequencies and bandwidths will be converted into periodogram bin numbers (k_{HS}, k_{LS}, k_{HN}, and k_{LN} in Fig. 9) and used by the DDP to compute the σ° cell power over the bandwidth.

IV. Discussion and Conclusions

In this paper, we have discussed general design issues for the onboard signal processor for spaceborne scatterometers. We then concentrated on the design of the onboard digital Doppler processor to be used by NSCAT.

The NSCAT digital Doppler processor will use digital signal processing techniques to process the scatterometer return signal into σ° cell power measurements. The FFT-based signal processing technique is designed to allow adjustment of the σ° cell Doppler center frequencies to compensate for the Earth's rotation. Computation of the adjustment to the cell center frequencies will be done onboard using an approximate expression for the Doppler shift of the cell center versus orbit time. This technique also permits modification of the parameters used to locate the σ° measurement cells by ground command in response to orbit changes. Real-time computation of the Doppler center frequencies will be done onboard the spacecraft.

In this paper, although we have concentrated on the digital Doppler processor for NSCAT, we feel that the design issues and tradeoffs considered during the design and analysis of the digital Doppler processor for NSCAT will be of general interest in the development of spaceborne scatterometers. We hope that the discussion of these design issues will be of value to the designers of other related radar remote-sensing instruments.

References

[1] F. Ulaby, R. Moore, and A. Fung, *Microwave Remote Sensing*, vols. 1-3. Dedham, MA: Artech House.

[2] E. M. Bracalente, D. H. Boggs, W. L. Grantham, and J. L. Sweet, "The SASS scattering coefficient (σ°) algorithm," *IEEE J. Ocean. Eng.*, vol. OE-5, Apr. 1980.

[3] J. Johnson, L. Williams, E. Bracalente, F. Beck, and W. Grantham, "SEASAT—A satellite scatterometer instrument evaluation," *IEEE J. Ocean. Eng.*, vol. OE-5, Apr. 1980.

[4] W. L. Grantham *et al.*, "Performance evaluation of an operational spaceborne scatterometer," *IEEE Trans. Geosci. Electron.*, vol. GE-20, no. 3, July 1982.

[5] F. Li, P. Callahan, M. Freilich, D. Long, and C. Winn, "NASA scatterometer for NROSS—A system for global oceanic wind measurement," *Proc. SPIE*, vol. 481, pp. 193-198, 1984.

[6] L. C. Schroeder, *et al.*, "Removal of ambiguous wind directions for a Ku-band wind scatterometer using three different azimuth angles," *IEEE Trans. Geosci. Remote Sensing*, vol. GE-23, no. 2, pp. 91-100, Mar. 1985.

[7] R. Fisher, "Standard deviation of scatterometer measurements from space," *IEEE Trans. Geosci. Electron.*, vol. GE-10, no. 2, Apr. 1972.

[8] C.-Y. Chi, D. Long, and F. Li, "Radar backscatter measurement accuracies using digital Doppler processors in spaceborne scatterometers," *IEEE Trans. Geosci. Remote Sensing*, vol. GE-24, no. 3, pp. 426-437, May 1986.

[9] J. J. O'Brien, Ed., *Scientific Opportunities Using Satellite Wind Stress Measurements over the Ocean*. Fort Lauderdale: NOVA Univ. N.Y.I.T. Press, 1982.

[10] A. Oppenheim and R. Schafer, *Digital Signal Processing*. Englewood Cliffs, NJ: Prentice-Hall, 1975.

[11] C.-Y. Chi, D. Long, and F. Li, "Roundoff noise analysis for digital signal power processors using Welch's power spectrum estimation," *IEEE Trans. Acoustics, Speech and Signal Processing*, vol. ASSP-35, no. 6, June 1987.

[12] ——, "Roundoff noise analysis for digital Doppler processors in radar scatterometers," presented at IGARSS, Zurich, Switzerland, Sept. 1986.

*

David G. Long received both the B.S. and M.S. degrees in electrical engineering from Brigham Young University, Provo, UT in 1982 and 1983, respectively. He is currently working toward the Ph.D. degree in electrical engineering at the University of Southern California, Los Angeles, CA.

He has been working for the Jet Propulsion Laboratory, Pasadena, CA, since May 1983 where he is a member of the technical staff in the Radar Science and Engineering section and is involved in the system design and analysis of spaceborne scatterometers. In 1985 he was awarded the NASA Award of Achievement for his work in computer graphics. His research interests include speech and digital signal processing, multidimensional signal processing, artificial intelligence, radar remote sensing, and computer graphics.

He has served as the vice president of a student chapter of IEEE and is currently a member of the IEEE Geoscience and Remote Sensing and the IEEE Acoustics, Speech and Signal Processing Societies. He is a member of the Tau Beta Pi, Eta Kappa Nu, and Sigma Xi honor societies.

*

Chong-Yung Chi (S'83-M'83) was born in Taiwan, Republic of China, on August 7, 1952. He received the B.S. degree from the Tatung Institute of Technology, Taipei, Taiwan, in 1975, the M.S. degree from the National Taiwan University, Taipei, Taiwan, in 1977, and the Ph.D. degree from the University of Southern California, Los Angeles, CA, in 1983, all in electrical engineering.

From September 1979 to June 1983 he was a Teaching/Research Assistant in the Department of Electrical Engineering-Systems at the University of Southern California. Since July 1983 he has been with Jet Propulsion Laboratory, Pasadena, CA. He has worked on spaceborne radar scatterometer systems to measure the global sea surface winds and the deconvolution of radar altimeter signals. Currently, he is working on SAR processor system design and simulations. His research interests include digital signal processing, radar imaging, deconvolution, adaptive filtering, system identification, and estimation theory.

*

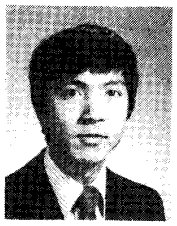

Fuk K. Li was born in Hong Kong in 1953. He received the B.Sc. and Ph.D. degrees in physics from the Massachusetts Institute of Technology, Cambridge, in 1975 and 1979, respectively.

He joined the Jet Propulsion Laboratory, California Institute of Technology, in 1979 and has been involved in various radar remote-sensing activities. He has developed a digital SAR processor/simulator, investigated the tradeoffs of various SAR image quality parameters, and developed several techniques for SAR Doppler parameter estimations. Since 1983, he has also been involved in the design and research studies of airborne and spaceborne scatterometers for remote sensing of ocean winds. He is at present the supervisor of the Radar System Science and Engineering Group. His group activities include: system design and engineering support for the NASA scatterometer, an airborne scatterometer and a rain mapping radar, system design for future spaceborne radars such as a Titan mapping radar, imaging altimeter, advanced scatterometer, etc., and electromagnetic scattering studies, especially those related to multipolarization SAR's.